

Unified Generative Adversarial Networks for Controllable Image-to-Image Translation

Hao Tang, Hong Liu and Nicu Sebe

Controllable image-to-image translation, i.e., transferring an image from a source domain to a target one guided by controllable structures, has attracted much attention in both academia and industry. In this paper, we propose a unified Generative Adversarial Network (GAN) framework for controllable image-to-image translation. In addition to conditioning on a reference image, we show how the model can generate images conditioned on controllable structures, e.g., class labels, object keypoints, human skeletons and scene semantic maps. The proposed GAN framework consists of a single generator and a discriminator taking a conditional image and the target controllable structure as input. In this way, the conditional image can provide appearance information and the controllable structure can provide the structure information for generating the target result. Moreover, the proposed GAN learns the image-to-image mapping through three novel losses, i.e., color loss, controllable structure guided cycle-consistency loss and controllable structure guided self-identity preserving loss. Note that the proposed color loss handles the issue of “channel pollution” when back-propagating the gradients. In addition, we present the Fréchet ResNet Distance (FRD) to evaluate the quality of generated images. Extensive qualitative and quantitative experiments on two challenging image translation tasks with four different datasets, i.e., hand gesture-to-gesture translation and cross-view image translation, demonstrate that the proposed GAN model generates convincing results, and significantly outperforms other state-of-the-art methods on both tasks. Meanwhile, the proposed GAN framework is a unified solution, thus it can be applied to solving other controllable structure guided image-to-image translation tasks, such as landmark-guided facial expression translation and keypoint-guided person image generation. To the best of our knowledge, we are the first to make one GAN framework work on all such controllable structure guided image translation tasks. The source code, data and trained models are available at <https://github.com/Ha0Tang/GestureGAN>.

Index Terms—Generative Models, Generative Adversarial Networks (GANs), Image-to-Image Translation, Controllable Structure, Hand Gesture-to-Gesture Translation, Cross-View Image Translation, Cycle-Consistency, Channel Pollution, Fréchet ResNet Distance

I. INTRODUCTION

GENERATIVE Adversarial Networks (GANs) [17] are generative models based on game theory, which have achieved impressive performance in a wide range of applications such as high-quality image generation [18], [19]. To generate specific kinds of images, Mirza et al. [20] propose Conditional GANs (CGANs), which comprise a vanilla GAN model and other external controllable structure information, such as class labels [16], reference images [2], object keypoints [21], [4], human skeletons [22], [8] and semantic maps [9], [23]

In this paper, we mainly focus on the image-to-image translation task using CGANs. At a high level, current image-to-image translation techniques usually fall into one of two types: supervised/paired [2], [24] and unsupervised/unpaired [11], [16]. However, existing image-to-image translation frameworks are inefficient for the multi-domain image-to-image translation task. For instance, given n different image domains, Pix2pix [2] and BicycleGAN [3] need to train $A_n^2 = n(n-1) = \Theta(n^2)$ models. CycleGAN [11], DiscoGAN [12] and DualGAN [13] need to train $C_n^2 = \frac{n(n-1)}{2} = \Theta(n^2)$ models, or $n(n-1)$ generator/discriminator pairs since one model has two different generator/discriminator pairs for these methods. ComboGAN [14] requires $n = \Theta(n)$ models. G²GAN [15] needs to train two

generators, i.e., the generation generator and the reconstruction generator, while StarGAN [16] only needs one model. However, for some specific image-to-image translation applications such as hand gesture-to-gesture translation [22] and person image generation [4], n could be arbitrary large since hand gestures and human bodies in the wild can have arbitrary poses, sizes, appearances, locations and self-occlusions.

To address these limitations, several works have been proposed to generate images based on controllable structures, e.g., object keypoints, human skeleton, and scene semantic maps. These works can be divided in three different categories: (i) Object keypoint guide methods. Reed et al. [21] proposed GAWWN, which generates bird images conditioned on bird keypoints. Song et al. [5] propose G2GAN for facial expression synthesis based on facial landmarks. Ma et al. propose PG² [4] and a two-stage reconstruction pipeline [6] achieving person image translation using a conditional image and a target pose image. (ii) Human skeleton guided methods. Siarohin et al. [8] introduce PoseGAN based on the human skeleton for human image generation. Tang et al. [22] propose a novel GestureGAN conditioned hand skeleton for hand gesture-to-gesture image translation task. Yan et al. [7] propose a method to generate human motion sequence with simple background using CGANs and human skeleton information. (iii) Scene semantic guide methods. Wang et al. [24] propose Pix2pixHD, which can be used for turning semantic label maps into photo-realistic images or synthesizing portraits from face label maps. Park et al. [23] propose the spatially-adaptive normalization, a simple but effective layer for synthesizing images given an input semantic layout. Regmi and Borji [10] propose X-

Hao Tang and Nicu Sebe are with the Department of Information Engineering and Computer Science (DISI), University of Trento, Trento 38123, Italy. E-mail: hao.tang@unitn.it, sebe@disi.unitn.it.

Hong Liu is with the Shenzhen Graduate School, Peking University, Shenzhen 518055, China. E-mail: hongliu@pku.edu.cn.

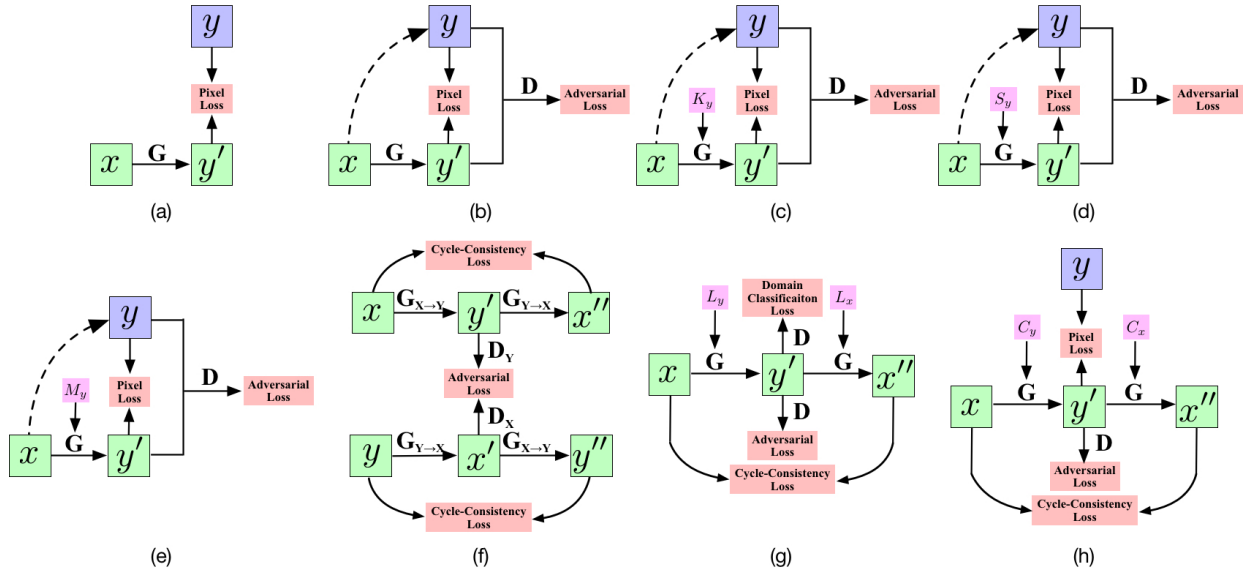


Fig. 1: Comparison with the state-of-the-art image-to-image translation methods. (a) Traditional deep learning methods, e.g., Context Encoder [1]. (b) Adversarial learning methods, e.g., Pix2pix [2] and BicycleGAN [3]. (c) Keypoint-guided image generation methods, e.g., PG² [4], G²GAN [5] and DPIG [6]. (d) Skeleton-guided image generation methods, e.g., SAMG [7] and PoseGAN [8]. (e) Semantic-guided image generation methods, e.g., SelectionGAN [9] and X-Fork [10]. (f) Adversarial unsupervised learning methods, e.g., CycleGAN [11], DiscoGAN [12] and DualGAN [13]. (g) Multi-domain image translation methods, e.g., ComboGAN [14], G²GAN [15] and StarGAN [16]. (h) Proposed GAN model in this paper. Note that the proposed GAN model is a unified solution for controllable structure guided image-to-image translation problem, i.e., controllable structure C can be one of class label L , object keypoint K , human skeleton S or semantic map M . Notations: x and y are the real images; x' and y' are the generated images; x'' and y'' are the reconstructed images; K_y is the keypoint of y ; S_y is the skeleton of y ; M_y is the semantic map of y ; L_x and L_y are the class labels of x and y , respectively; C_x and C_y are the controllable structures of x and y , respectively; G , $G_{X \rightarrow Y}$ and $G_{Y \rightarrow X}$ represent generators; D , D_Y and D_X denote discriminators.

Fork and X-Seq, which aim to generate images across two drastically different views by using the guidance of semantic maps.

The aforementioned methods have achieved impressive results on the corresponding tasks. However, each of them is tailored for a specific application limiting their capability to generalize. Our framework does not impose any application-specific constraint. This makes our setup considerably simpler than the other approaches see (Fig. 1). To achieve this goal, we propose a unified solution for controllable image-to-image translation. It allows generating high-quality images with arbitrary poses, sizes, structures and locations in the wild. Our GAN model only consists of one generator and one discriminator, taking a conditional image and the novel controllable structures as inputs. In this way, the conditional image can provide appearance information and the controllable structures can provide structure information for generating the target image. In addition, to better learn the mapping between inputs and outputs, we propose three novel losses, i.e., color loss, controllable structure guided cycle-consistency loss and self-identity preserving loss. The proposed color loss can handle the problem of “channel pollution” that is frequently occurring in generative models such as PG² [4], leading the generated images to be sharper and having higher quality. The proposed controllable structure guided cycle-consistency loss is more flexible than the one proposed in CycleGAN [11], reducing further the space of possible mappings between

different domains. The proposed self-identity preserving loss can improve the identity information and structure accuracy of the generated images. These optimization loss functions and the proposed GAN framework are jointly trained in an end-to-end fashion to improve both fidelity and visual naturalness of the generated images. Furthermore, we propose the Fréchet ResNet Distance (FRD), which is a novel and better evaluation metric to evaluate the generated images of GANs. Extensive experiments on two challenging controllable image-to-image translation tasks with four different datasets, i.e., hand gesture-to-gesture translation and cross-view image translation, demonstrate that the proposed GAN model generates high-quality images with convincing details and achieves state-of-the-art performance on both tasks. Finally, the proposed GAN model is a general-purpose solution that can be applied to solve a wide variety of controllable structure guided image-to-image translation problems.

In summary, the contributions of this paper are as follows:

- We propose a unified GAN model for controllable image-to-image translation tasks, which can generate target images with arbitrary poses, sizes, structures and locations in the wild.
- We propose three novel objective functions to better optimize the proposed GAN model, i.e., color loss, controllable structure guided cycle consistency loss and self-identity preserving loss. These optimization functions and the proposed GAN framework are jointly trained in an end-to-end fashion

to improve both quality and fidelity of the generated images.

- We propose an efficient Fréchet ResNet Distance (FRD) metric to evaluate the similarity of the real and generated images, which is more consistent with human judgment.
- Qualitative and quantitative results demonstrate the superiority of the proposed GAN model over the state-of-the-art methods on two challenging controllable image translation tasks with four datasets, i.e., hand gesture-to-gesture translation and cross-view image translation.

In the remainder of this paper, we first discuss related work in Sec. II. We then introduce the proposed unified GAN framework in Sec. III. In Sec. IV, extensive experiments on two challenging generative tasks with four different datasets are conducted to evaluate the proposed GAN framework and methods. Finally, conclusions are provided in Sec. V.

II. RELATED WORK

Generative Adversarial Networks (GANs) are unsupervised learning methods and have been proposed in [17]. Recently, GANs have shown promising results in various applications, e.g., image generation [18], [19], video generation [25], [26] and texture synthesis [27]. Recent approaches employ the idea of GANs for conditional image generation, such as image-to-image translation [2], text-to-image translation [28] and sketch generation [29], [30]. The key success of GANs is the adversarial loss, which allows the model to generate images that are indistinguishable from real image, and this is exactly the goal that many tasks aim to optimize. In this paper we mainly focus on image-to-image translation tasks.

Image-to-Image Translation is the problem of transferring an image from a source domain to a target domain, which uses input-output data to learn a parametric mapping between inputs and outputs, e.g., Isola et al. [2] propose Pix2pix, which uses a conditional GAN to learn a translation function from input to output image domains. Wang et al. [24] present a method for synthesizing high-resolution photo-realistic images from semantic label maps using CGANs. Both methods are trained on paired training data. However, collecting large sets of image pairs is often prohibitively expensive or unfeasible. To solve this limitation, Zhu et al. [11] propose CycleGAN, which can learn to translate between domains without paired input-output examples by using the cycle consistency loss. Similar ideas have been proposed in several works [13], [16], [15]. For example, Choi et al. [16] introduce StarGAN, which can perform image-to-image translation for multiple domains.

However, existing image-to-image translation models are inefficient and ineffective. For example, with n image domains, CycleGAN [11], DiscoGAN [12], and DualGAN [13] need to train $2C_n^2 = n(n-1) = \Theta(n^2)$ generators and discriminators, while Pix2pix [2] and BicycleGAN [3] have to train $A_n^2 = n(n-1) = \Theta(n^2)$ generator/discriminator pairs. Recently, Anoosheh et al. propose ComboGAN [14], which only needs to train n generator/discriminator pairs for n different image domains, having a complexity of $\Theta(n)$. Tang et al. [15] propose G²GAN, which can perform image-to-image translations for multiple domains using only two generators, i.e., the generation generator and the reconstruction generator.

Additionally, Choi et al. [16] propose StarGAN, in which a single generator and a discriminator can perform unpaired image-to-image translations for multiple domains. Although the computational complexity of StarGAN is $\Theta(1)$, this model has only been validated on the face attributes modification task with clear background and face cropping. More importantly, for some specific image-to-image translation tasks such as hand gesture-to-gesture translation [22] and person image generation [4] tasks, the image domains could be arbitrary large, e.g., hand gestures and human bodies in the wild can have arbitrary poses, sizes, appearances, structures, locations and self-occlusions. The aforementioned approaches are not effective for solving these specific situations.

Controllable Image-to-Image Translation. To fix these limitations, several recent works have been proposed to generate persons, birds, faces and scene images based on controllable structures, i.e., object keypoints [21], [4], [6], human skeletons [7], [8], [22], [31] and semantic maps [24], [9], [23], [10]. In this way, controllable structures provide four type of information to guide the image generation process, i.e., shape, scale, orientation and location. Although significant efforts have been made to achieve controllable image-to-image translation in the area of computer vision, there has been very limited research on universal controllable image translation. That is, the typical problem with the aforementioned generative models is that each of them is tailored for a specific application, which greatly limits the generalization ability of the proposed models. To handle this problem, we propose a novel and unified GAN model, which can be tailored for handling all kinds of problem settings of controllable structure guided image-to-image translation, including object keypoint guided generative tasks, human skeleton guided generative tasks and semantic map guided generative tasks, etc.

III. MODEL DESCRIPTION

In this section we present the details of the proposed GAN model (Fig. 2). We present a controllable structure guided generator, which utilizes the images from one domain and conditional controllable structures from another domain as inputs, and produce images in the target domain. Moreover, we propose a novel discriminator which also takes the controllable structure in consideration. The proposed GAN model is trained in an end-to-end fashion mutually benefiting from the generator and the discriminator.

A. Controllable Structure Guided Generator

Controllable Structure Guided Generation. Image-to-image translation tasks, such as hand gesture-to-gesture translation [22], person image generation [4], facial expression-to-expression translation [31] and cross-view image translation [10] are very challenging. In these tasks, the source domain and the target domain may have large deformations. Moreover, these tasks can be treated as an infinite mapping problem leading to ambiguity issues in the translation process. For instance, in hand gesture-to-gesture translation task, if you input a hand gesture image to the generator, it has no idea which gestures should output.

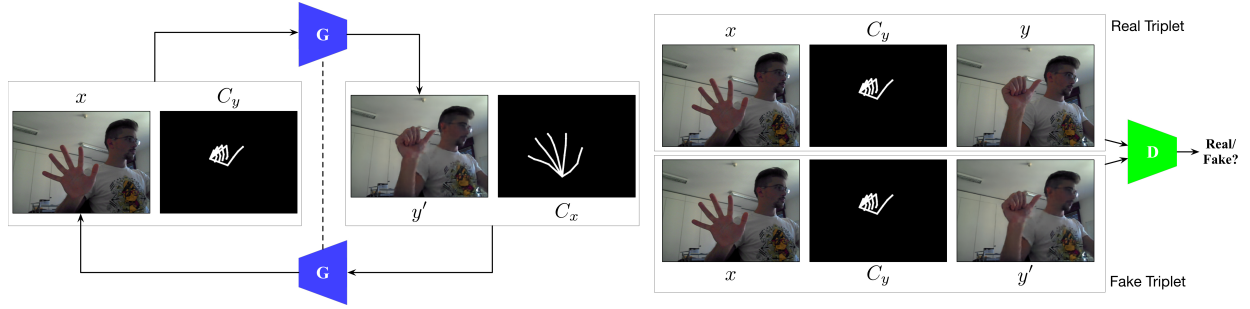


Fig. 2: Pipeline of the proposed unified GAN model for controllable image-to-image translation tasks. The proposed GAN framework consists of a single generator G and an associated adversarial discriminator D , which takes a conditional image x and a controllable structure C_y as input to produce the target image y' . We have two cycles and here we only show one of them. Note that the controllable structure C_y can be a class label, object keypoints, human skeletons, semantic maps, etc.

To fix this limitation, we employ controllable structures as the conditional guidance to guide the image generation process. The controllable structures can be class labels, object keypoints, human skeletons or semantic maps, etc. Following [4], [8], [10] we generate the controllable structures using deep models pretrained from other large-scale datasets, e.g., we apply the pose estimator OpenPose [32] to obtain approximate human body poses and hand skeletons. Specifically, as shown in Fig. 2, we concatenate the input conditional image x from the source domain and the controllable structure C_y from a target domain, and input them into the generator G and synthesize the target image $y'=G(x, C_y)$. In this way, the ground-truth controllable structure C_y provides stronger supervision and structure information to guide the image-to-image translation in the deep network, while the conditional image x provides the appearance information to produce the final result y' .

Controllable Structure Guided Cycle. Guided by the controllable structure C_y , our generator can produce the corresponding image y' . However, state-of-the-art controllable image-to-image translation methods such as [4], [8], [9], [10] only consider the image translation process, i.e., from the source domain to the target domain. Different from them, we consider both image translation process and image reconstruction process, i.e., from the source domain to the target domain and from the target domain back to the source domain. The intuition behind this is that if we translate from one domain to the other and back again we should arrive at where we started. The proposed controllable structure guided cycle is different from the cycle proposed in CycleGAN [11], which uses a cycle consistency loss to preserve the content of its input images while changing only the domain-related part of the inputs. The main difference is that CycleGAN can only handle two different domains, while an image translation problem such as hand gesture-to-gesture translation task has arbitrary domains, e.g., hand gestures in the wild can have arbitrary poses, sizes, appearances, structures, locations and self-occlusions. Therefore, we need the controllable structure to guide the learning of the proposed cycle. The proposed controllable structure guided cycle is also different from the cycle proposed in StarGAN [16], which translates an original image into an image in the target domain and then reconstructs the original image from the translated image through feeding the target

label. However, class labels can only provide the category information, while the controllable structure can provide four types of information for generation at the same time, i.e., category, location, scale and orientation. More specifically, as shown in Fig. 2, the generated image y' and the controllable structure C_x are concatenated to input into the generator G . The proposed controllable structure guided cycle can be formulated as follows,

$$x'' = G(y', C_x) = G(G(x, C_y), C_x) \approx x. \quad (1)$$

Note that we use a single generator twice, first to translate an original image into an image in the target domain and then to reconstruct the original image from the translated image. Image translation and image reconstruction are simultaneously considered in our framework, constructing a full mapping cycle. Similarly, we have another cycle,

$$y'' = G(x', C_y) = G(G(y, C_x), C_y) \approx y. \quad (2)$$

Controllable Structure Guided Cycle Consistency Loss.

To better optimize the proposed cycle, we propose a novel controllable structure guided cycle consistency loss. It is worth noting that CycleGAN [11] is different from the Pix2pix model [2] as the training data in CycleGAN is unpaired. CycleGAN introduces the cycle consistency loss to enforce forward-backward consistency. In that case, the cycle consistency loss can be regarded as “pseudo” pairs of training data even though we do not have the corresponding data in the target domain which corresponds to the input data from the source domain. However, in this paper we introduce the controllable structure guided cycle consistency loss for the paired image-to-image translation task. This loss ensures the consistency between source images and the reconstructed image, and it can be expressed as,

$$\mathcal{L}_{cyc}(G, C_x, C_y) = \mathbb{E}_{x, C_x, C_y} [\|x - G(G(x, C_y), C_x)\|_1] + \mathbb{E}_{x, C_x, C_y} [\|y - G(G(y, C_x), C_y)\|_1], \quad (3)$$

where G is the generator; x and y are the input images; C_x and C_y are the controllable structures of image x and y , respectively. As mentioned before, we use the same generator G twice. Equipped with this loss, the proposed generator G further improves the image quality due to its implicit data augmentation effect from a multi-task learning setting.



Fig. 3: Illustration of the “channel pollution” issue. From left to right: input image, ground truth, PG² [4] and ours.

B. Controllable Structure Guided Discriminator

Conditional GANs (CGANs) such as Pix2pix [2] learn the mapping $G(x) \mapsto y$, where x is the input conditional image. Generator G is trained to generate image y' that cannot be distinguished from “real” image y by an adversarially trained discriminator D , while the discriminator D is trained as well as possible to detect the “fake” images generated by the generator G . The objective function of CGANs is defined as follows,

$$\mathcal{L}_{cGAN}(G, D) = \mathbb{E}_{x,y} [\log D(x, y)] + \mathbb{E}_x [\log(1 - D(x, G(x)))], \quad (4)$$

where generator G tries to minimize this objective function while the discriminator D tries to maximize it. Thus, the solution is $G^* = \arg \min_G \max_D \mathcal{L}_{cGAN}(G, D)$. In this paper, we try to learn two mappings through one generator, i.e., $G(x, C_y) \mapsto y$ and $G(y', C_x) \mapsto x$. As shown in Fig. 2, in order to learn both mappings, we employ the controllable structures explicitly. Thus, the adversarial losses of the two mappings are defined respectively, as follows:

$$\mathcal{L}_{adv}(G, D, C_y) = \mathbb{E}_{[x, C_y], y} [\log D([x, C_y], y)] + \mathbb{E}_{[x, C_y]} [\log(1 - D([x, C_y], G(x, C_y)))], \quad (5)$$

where C_y is the controllable structure of image y and $[\cdot, \cdot]$ represents the concatenation operation. This controllable structure guided input encourages D to capture the local-aware information and generate semantic-matched target images. Similarly, we have another adversarial loss,

$$\mathcal{L}_{adv}(G, D, C_x) = \mathbb{E}_{[y, C_x], x} [\log D([y, C_x], x)] + \mathbb{E}_{[y, C_x]} [\log(1 - D([y, C_x], G(y, C_x)))]. \quad (6)$$

Thus, the final adversarial loss is the sum of Eq. (5) and (6),

$$\mathcal{L}_{adv}(G, D) = \mathcal{L}_{adv}(G, D, C_x) + \mathcal{L}_{adv}(G, D, C_y). \quad (7)$$

C. Optimization Objective

Color Loss. Previous work indicates that mixing the adversarial loss with a traditional loss such as $L1$ loss [2] or $L2$ loss [1] between the generated images and the ground truth images improves the generation performance. The definitions of $L1$ and $L2$ losses are:

$$\mathcal{L}_{L\{1,2\}}(G) = \mathbb{E}_{[x, C_y], y} [\|y - G([x, C_y])\|_{\{1,2\}}] + \mathbb{E}_{[y, C_x], x} [\|x - G([y, C_x])\|_{\{1,2\}}]. \quad (8)$$

However, we observe that the existing image-to-image translation models such as PG² [4] cannot retain the holistic color of the input images. An example is shown in Fig. 3, where PG² is affected by the pollution issue and produces more unrealistic regions. Therefore, to address this limitation we introduce a novel channel-wise color loss. Traditional generative models convert an entire image into another, which leads to the

“channel pollution” problem. However, the color loss treats r , g and b channels independently and generates only one channel each time, and then these three channels are combined to produce the final image. Intuitively, since the generation of a three-channel image space is much more complex than the generation of a single-channel image space, leading to higher possibility of artifacts, we independently generate each channel. The objective of r , g and b channel losses can be defined as follows,

$$\mathcal{L}_{color_{c\{1,2\}}}(G) = \mathbb{E}_{[x_c, C_y], y_c} [\|y_c - G([x_c, C_y])\|_{\{1,2\}}] + \mathbb{E}_{[y_c, C_x], x_c} [\|x_c - G([y_c, C_x])\|_{\{1,2\}}]. \quad (9)$$

where $c \in \{r, g, b\}$; x_r , x_g and x_b denote the r , g and b channels of image x respectively similar to y_r , y_g and y_b ; $\|\cdot\|_1$ and $\|\cdot\|_2$ represent $L1$ and $L2$ distance losses. Thus, the color $L1$ and $L2$ losses can be expressed as,

$$\mathcal{L}_{color\{1,2\}}(G) = \mathcal{L}_{Color_r\{1,2\}} + \mathcal{L}_{Color_g\{1,2\}} + \mathcal{L}_{Color_b\{1,2\}}. \quad (10)$$

In Eq. (8), one channel is always influenced by the errors from other channels. On the contrary, if we compute the loss for each channel independently as shown in Eq. (10), we can avoid such influence. In this way, the error in one channel will not influence other channels. We observe that this novel loss can improve the image quality in our experimental section.

Controllable Structure Guided Self-Identity Preserving Loss.

To preserve the identity information between the input and output, CycleGAN [11] proposes the identity preserving loss. However, different from them, we propose the controllable structure guided self-identity preserving loss, which can be expressed as follows,

$$\mathcal{L}_{id}(G) = \mathbb{E}_{x, C_x} [\|x - G(x, C_x)\|_1] + \mathbb{E}_{y, C_y} [\|y - G(y, C_y)\|_1]. \quad (11)$$

We minimize the $L1$ difference between the real image x/y and the self-identity preserving image $G(x, C_x)/G(y, C_y)$ for identity preservation. In this way, we regularize the generator to be near a self-identity mapping when real images and self controllable structure are provided as the input to the generator.

Perceptual Loss measures the perceptual similarity in a high-level feature space. This loss has been shown to be useful for many tasks such as style transfer [33] and image translation [24]. The formulation of this loss is as follows:

$$\mathcal{L}_{vgg}(y') = \frac{1}{W_{i,j} H_{i,j}} \sum_{w=1}^{W_{i,j}} \sum_{h=1}^{H_{i,j}} \|\mathcal{F}^k(y) - \mathcal{F}^k(G(x, C_y))\|_1, \quad (12)$$

where \mathcal{F}^k indicates the feature map obtained by the k -th convolution within the VGG network [34], $W_{i,j}$ and $H_{i,j}$ are the dimensions of the respective feature maps within the VGG network. Similarly, we have another loss for the generated image x' and the final perceptual loss is the sum of both.

Total Variation Loss. Usually, the images synthesized by GAN models have many unfavorable artifacts, which deteriorate the visualization and the recognition performance. We impose a Total Variation (TV) loss [33] on the final

synthesized image y' to alleviate this issue,

$$\mathcal{L}_{tv}(y') = \sum_{c=1}^C \sum_{w,h=1}^{W,H} |y'(w+1, h, c) - y'(w, h, c)| + |y'(w, h+1, c) - y'(w, h, c)|, \quad (13)$$

where W and H represent the width and height of the generated image y' . Similarly, we have another loss for the generated image x' and the final total variation loss is the sum of both.

Overall Loss. The total optimization loss is a weighted sum of the above losses. Generator G and discriminator D are trained in an end-to-end fashion to optimize the following min-max function,

$$G^* = \arg \min_G \max_D (\mathcal{L}_{adv} + \lambda_{color} \mathcal{L}_{color} + \lambda_{cyc} \mathcal{L}_{cyc} + \lambda_{id} \mathcal{L}_{id} + \lambda_{vgg} \mathcal{L}_{vgg} + \lambda_{tv} \mathcal{L}_{tv}), \quad (14)$$

where λ_{color} , λ_{cyc} , λ_{id} , λ_{vgg} and λ_{tv} are five hyper-parameters controlling the relative importance of these six losses. Solving this min-max problem enables our model to generate the target images guided by controllable structures in a photo-realistic manner.

D. Implementation Details

Network Architecture. We adopt our generator architecture G from [33], which has shown effective in many applications such as unsupervised image translation [11] and neural style transfer [33]. We use nine residual blocks for both 64×64 and 256×256 image resolutions. The last layer of the generator is the Tanh activation function. For the discriminator D , we adopt 70×70 PatchGAN proposed in [2]. PatchGAN tries to decide if any 70×70 patch in an image is real or fake. The final layer of discriminators employ the Sigmoid activation function to produce a 1-dimensional output. Therefore, we are averaging all responses to provide the ultimate output of the discriminator.

Optimization Details. We observe that the proposed controllable structure guided discriminator achieves promising generation results. However, to further improve the image quality, we use the scheme of training a dual-discriminator instead of one discriminator as a more stable way to improve the capacity of discriminators similar to Nguyen et al. [35], which have demonstrated that they improve the ability of discriminator to generate more photo-realistic images. To be more specific, the dual-discriminator architecture can better approximate the optimal discriminator. If one of the discriminators is trained to be far superior over the generators, the generators can still receive instructive gradients from the other one. In addition to the proposed controllable structure guided discriminator, we use a traditional one, which takes the input image and the generated image as input. Both discriminators have the same network architecture structure.

We follow the standard optimization method in [17], [2] to optimize the proposed GAN model, i.e., one gradient descent step on discriminators and generator alternately. We first train generator G with discriminators fixed, and then train discriminators with generator G fixed. In addition, as

suggested in [17], we train to maximize $\log D([x, C_y], y')$ rather than $\log(1 - D([x, C_y], y'))$. Moreover, in order to slow down the rate of D relative to G we divide the objective function by 2 while optimizing D . The proposed GAN model is trained and optimized in an end-to-end fashion. We employ the Adam [36] optimizer with momentum terms $\beta_1=0.5$ and $\beta_2=0.999$ as our solver. The initial learning rate for Adam is 0.0002.

We follow [4] and exploit OpenPose [37] to detect the ground-truth hand skeletons as training data for the hand gesture-to-gesture translation task. We then connect the 21 keypoints (hand joints) detected by OpenPose to obtain the hand skeleton. The hand skeleton image visually contains richer hand structure information than the hand keypoint image. In hand skeleton images, the hand joints are connected by the lines with the width of 4 and with white color. In addition, we follow [10] and use RefineNet [38] to generate the ground-truth semantic maps as training data for the cross-view image translation task.

IV. EXPERIMENTS

To explore the generality of the proposed GAN model, we evaluate the proposed model on a variety of tasks and datasets, including hand gesture-to-gesture translation task and cross-view image translation task.

A. Experimental Setup

Datasets. (i) For hand gesture-to-gesture translation task, we follow GestureGAN [22] and evaluate the proposed GAN model on two hand gesture datasets, i.e., NTU Hand Digit [39] and Creative Senz3D [40], which include different hand gestures. We use the hand gesture images and filter out failure cases in hand estimation for both training and testing sets. (1) NTU Hand Digit dataset [39] contains 10 hand gestures (e.g., decimal digits from 0 to 9) color images and depth maps collected with a Kinect sensor under cluttered background. We randomly select 84,636 pairs, each of which is comprised of two images of the same person but different gestures. 9,600 pairs are randomly selected for the testing subset and the rest of 75,036 pairs as the training set; (2) Creative Senz3D dataset [40] includes static hand gestures performed by 4 people, each performing 11 different gestures repeated 30 times each in the front of a Creative Senz3D camera. We randomly select 12,800 pairs and 135,504 pairs as the testing and training set, each pair being composed of two images of the same person but different gestures.

(ii) For cross-view image translation task, we follow [10] and conduct the experiments on two public datasets: (1) For the Dayton dataset [41], following the same setting of [10], we select 76,048 images and create a train/test split of 55,000/21,048 pairs. The images in the original dataset have 354×354 resolution. We resize them to 256×256 ; (2) The CVUSA dataset [42] consists of 35,532/8,884 image pairs in train/test split. Following [10], the aerial images are center-cropped to 224×224 and resized to 256×256 . For the ground level images and corresponding segmentation maps, we take the first quarter of both and resize them to 256×256 ;

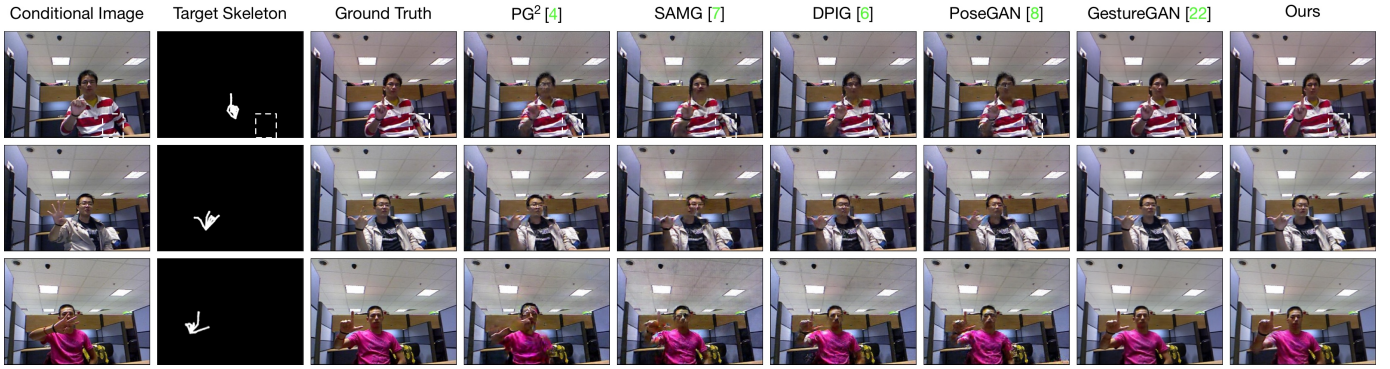


Fig. 4: Different methods for hand gesture-to-gesture translation task on NTU Hand Digit dataset.

TABLE I: Ablation study of the proposed GAN model on Dayton dataset for cross-view image translation task. For all evaluation metrics except KL and LPIPS, higher is better.

Baseline	Experimental Setting	SSIM ↑	PSNR ↑	SD ↑	Accuracy ↑				KL ↓	LPIPS ↓
					Top-1	Top-5				
A	$x \xrightarrow{G} y'$ (Unsupervised Learning)	0.4110	17.9868	18.5195	27.28	47.47	52.47	71.63	8.69±1.36	0.5913
B	$x \xrightarrow{G} y'$ (Supervised Learning)	0.4555	19.6574	18.8870	27.46	46.84	58.20	77.17	6.25±1.30	0.5520
C	$[x, C_x] \xrightarrow{G} y'$ (Controllable Structure Guided Generation)	0.5374	22.8345	19.2075	39.76	68.44	72.22	89.85	3.32±1.10	0.4010
D	$[x, C_y] \xrightarrow{G} [y', C_x] \xrightarrow{G} x'$ (Controllable Structure Guided Cycle)	0.5547	23.1531	19.6032	42.43	70.82	75.40	91.16	2.89±1.05	0.3821
E11	D + Color L1 Loss on x'	0.5515	23.1345	19.6257	-	-	-	-	-	-
E12	D + Color L1 Loss on y'	0.5600	23.3692	19.7018	-	-	-	-	-	-
E13	D + Color L2 Loss on y' + L1 loss on y'	0.5568	23.3930	19.6273	-	-	-	-	-	-
E14	D + Color L1 Loss on y' + L1 loss on y'	0.5631	23.4600	19.7650	-	-	-	-	-	-
E21	D + Controllable Structure Guided Discriminator	-	-	-	43.08	72.80	74.98	90.89	-	-
E22	D + Dual Discriminator	-	-	-	43.12	74.85	76.14	91.23	-	-
E3	D + Controllable Structure Guided Self-Identity Preserving Loss	-	-	-	-	-	-	-	2.76±0.99	-
E41	D + Perceptual Loss	-	-	-	-	-	-	-	-	0.3545
E42	D + Perceptual Loss + Total Variation Loss	-	-	-	-	-	-	-	-	0.3543
F	D + E14 + E22 + E3 + E42	0.5603	23.1626	19.7455	46.43	76.94	79.54	94.33	2.35±0.84	0.3571

Parameter Settings. (i) Hand gesture-to-gesture translation task: for both datasets, we do left-right flip and random crops for data augmentation. For optimization, models are trained with a batch size of 4 for 20 epochs on both datasets. At inference time, we follow the same settings of PG² [4] to randomly select the target keypoint or skeleton. (ii) Cross-view image translation: for a fair comparison, we follow [10] and all images are scaled to 256×256, and we enabled random crops for data augmentation. Similar to [10], the low resolution experiments on Dayton dataset are carried out for 100 epochs with batch size of 16, whereas the high resolution experiments for this dataset are trained for 35 epochs with batch size of 4. For CVUSA dataset, we follow the same setup as in [10] and train our network for 30 epochs with batch size of 4. The proposed GAN model is implemented using the public deep learning framework PyTorch. We perform our experiments on two NVIDIA TITAN Xp GPUs with 12G memory to accelerate both training and inference.

Evaluation Metrics. For fair comparison, here we use several measures to evaluate our methods on both tasks. (i) Hand gesture-to-gesture translation task: following GestureGAN [22], Peak Signal-to-Noise Ratio (PSNR), Inception Score (IS), Fréchet Inception Distance (FID) and user study (AMT score) are employed to evaluate the quality of generated images. (ii) Cross-view image translation: we follow [10] and use Inception Score (IS), top-k prediction accuracy, KL score, Structural-Similarity (SSIM), PSNR and Sharpness Difference (SD) for the quantitative analysis.

Beside these metrics, we also propose a novel evaluation

metric to measure the image quality of the generated images by GAN models, i.e., Fréchet ResNet Distance (FRD). FRD provides an alternative method to quantify the quality of synthesis and is similar to the FID proposed by [43]. FID is a measure of similarity between two datasets of images. The authors have shown that the FID is more robust to noise than IS and correlates well with the human judgment of visual quality [43]. To calculate FID between two image domains y and y' , they first embed both into a feature space F given by an Inception model. Then viewing the feature space as a continuous multivariate Gaussian as suggested in [43], Fréchet distance between the two Gaussians is used to quantify the quality of the data. The definition of FID is:

$$\text{FID}(y, y') = \|\mu_y - \mu_{y'}\|_2^2 + \text{Tr}(\sum_y + \sum_{y'} - 2(\sum_y \sum_{y'})^{\frac{1}{2}}), \quad (15)$$

where (μ_y, \sum_y) and $(\mu_{y'}, \sum_{y'})$ are the mean and the covariance of the data distribution and model distribution, respectively.

Unlike FID, which regards the datasets y and y' as a whole, the proposed FRD is inspired from feature matching methods [44], and separately calculates the Fréchet distance between generated images and real images from the semantical level. In this way, images from two domains do not affect each other when computing the Fréchet distance. Moreover, for FID the number of samples should be greater than the dimension of the coding layer, while the proposed FRD does not have this limitation. We denote y_i and y'_i as images in the y and y' domains, respectively. For calculating FRD, we



Fig. 5: Different methods for hand gesture-to-gesture translation task on Senz3D dataset.
TABLE II: The influence of λ_{cyc} on Dayton dataset for cross-view image translation task.

λ_{cyc}	SSIM \uparrow	PSNR \uparrow	SD \uparrow	Inception Score \uparrow			Accuracy \uparrow				KL \downarrow	LPIPS \downarrow
				all	Top-1	Top-5	Top-1		Top-5			
100	0.5383	23.0283	19.5731	2.9278	1.9960	2.9823	39.22	67.86	69.55	88.03	3.96 ± 1.32	0.4082
10	0.5475	23.1264	19.5590	3.2344	2.2321	3.2983	42.30	67.99	74.98	89.54	2.87 ± 1.01	0.3832
1	0.5478	23.1153	19.5158	3.1918	2.2025	3.2362	42.11	72.26	75.37	91.33	2.88 ± 1.02	0.3869
0.1	0.5547	23.1731	19.6032	3.2823	2.2401	3.3081	42.43	70.82	75.40	91.16	2.89 ± 1.05	0.3821

TABLE III: The influence of λ_{id} on Dayton dataset for cross-view image translation task.

λ_{id}	0.1	1	5	10	100
KL \downarrow	2.85 ± 1.03	2.93 ± 1.00	2.83 ± 1.01	3.00 ± 1.02	2.76 ± 0.99

TABLE IV: The influence of λ_{vgg} on Dayton dataset for cross-view image translation task.

λ_{vgg}	1	10	20	50	100
LPIPS \downarrow	0.3812	0.3708	0.3628	0.3571	0.3545

TABLE V: The influence of the number of cycles on NTU Hand Digit dataset for hand gesture-to-gesture translation task.

# Cycle	PSNR \uparrow	IS \uparrow	FID \downarrow	FRD \downarrow
One-Cycle	30.4531	2.1898	13.9475	2.2176
Two-Cycle	31.4924	2.1493	11.2084	2.0774

first embed both images y_i and y'_i into a feature space F with 1,000 dimension given by a ResNet pretrained model. We then calculate the Fréchet distance between two feature maps $f(y_i)$ and $f(y'_i)$. The Fréchet distance $F(f(y_i), f(y'_i))$ is defined as the infimum over all reparameterizations α and β of $[0, 1]$ of the maximum over all $t \in [0, 1]$ of the distance in F between $f(y_i)(\alpha(t))$ and $f(y'_i)(\beta(t))$, where α and β are continuous, non-decreasing surjections of the range $[0, 1]$. The proposed FRD is a measure of similarity between the feature vector of the real image $f(y_i)$ and the feature vector of the generated image $f(y'_i)$ by calculating the Fréchet distance between them. The Fréchet distance is defined as the minimum cord-length sufficient to join a point traveling forward along $f(y'_i)$ and one traveling forward along $f(y_i)$, although the rate of travel for each point may not necessarily be uniform. Thus, the definition of FRD between two image domains y and y' is:

$$\text{FRD}(y, y') = \frac{1}{N} \sum_1^N \inf_{\alpha, \beta} \max_{t \in [0, 1]} \{d(f(y_i)(\alpha(t)), f(y'_i)(\beta(t)))\}, \quad (16)$$

where d is the distance function of F and N is the total number

of images in y and y' domains.

B. Ablation Study

We perform an ablation study in the a2g (aerial-to-ground) direction on Dayton dataset for the cross-view image translation task. Following [9], to reduce the training time, we randomly select 1/3 samples from the whole 55,000/21,048 samples, i.e., around 18,334 samples for training and 7,017 samples for testing.

Baseline Models. The proposed GAN model has nine baselines (A, B, C, D, E1x, E2x, E3, E4x, F) as shown in Table I. Baseline A uses a CycleGAN model [11] and generates y' using an unpaired image x . Baseline B uses a Pix2pix structure [2], and generates y' based on x using a supervised way. Baseline C also uses Pix2pix structure, and inputs the combination of a conditional image x and the controllable structure C_y to the proposed controllable structure guided generator G . Baseline D uses the proposed controllable structure guided cycle upon baseline C. Baseline E1x explore the proposed color loss in several different ways to avoid the “channel pollution” issue. Baseline E2x employ the proposed controllable structure guided discriminator to stabilize the optimization process. Baseline E3 adds the proposed controllable structure guided self-identity preserving loss to preserve the identity information. Baseline E4x adds the perceptual loss and the total variation loss on the generated result y' . Baseline F is our final full model integrating baselines D, E14, E22, E3 and E42. All the baseline models are trained and tested on the same data using the same configuration.

Note that each baseline in E (i.e., E1x, E2x, E3 and E4x) focuses on improving each aspect of the performance of the generated images. More specifically, the proposed color loss aims to avoid the “channel pollution” issue and thus improve the pixel-level similarity metrics, i.e., SSIM, PSNR and SD. The proposed controllable structure guided discriminator tries

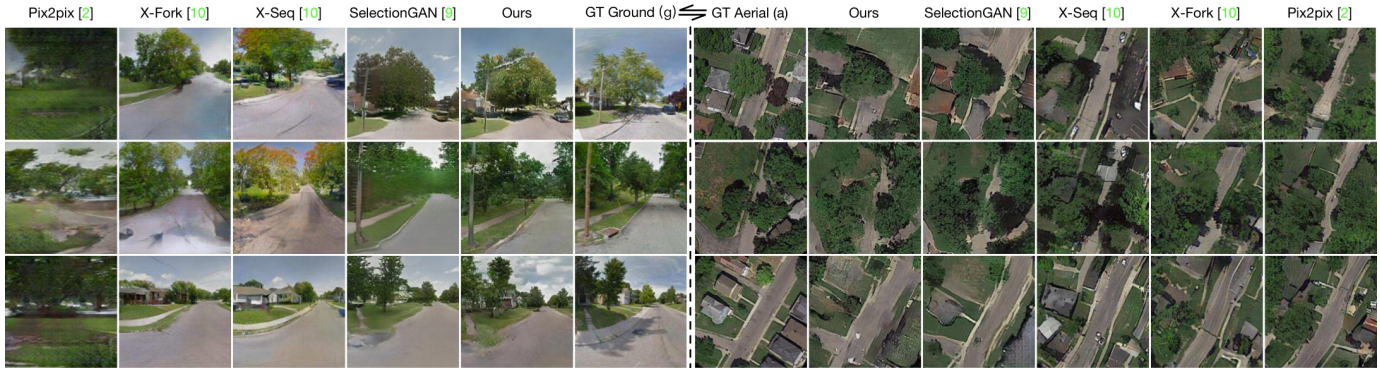


Fig. 6: Different methods for cross-view image translation task in 256×256 resolution on Dayton dataset.

TABLE VI: Comparison results with state-of-the-art models for hand gesture-to-gesture translation task on both NTU Hand Digit and Senz3D datasets. For all metrics except FID and FRD, higher is better. (*) These results are reported in [22].

Method	NTU Hand Digit					Senz3D				
	PSNR \uparrow	IS \uparrow	AMT \uparrow	FID \downarrow	FRD \downarrow	PSNR \uparrow	IS \uparrow	AMT \uparrow	FID \downarrow	FRD \downarrow
PG ² [4]	28.2403*	2.4152*	3.5%*	24.2093*	2.6319*	26.5138*	3.3699*	2.8%*	31.7333*	3.0933*
SAMG [7]	28.0185*	2.4919*	2.6%*	31.2841*	2.7453*	26.9545*	3.3285*	2.3%*	38.1758*	3.1006*
DPIG [6]	30.6487*	2.4547*	7.1%*	6.7661*	2.6184*	26.9451*	3.3874*	6.9%*	26.2713*	3.0846*
PoseGAN [8]	29.5471*	2.4017*	9.3%*	9.6725*	2.5846*	27.3014*	3.2147*	8.6%*	24.6712*	3.0467*
GestureGAN [22]	32.6091*	2.5532*	26.1%*	7.5860*	2.5223*	27.9749*	3.4107*	22.6%*	18.4595*	2.9836*
Ours	32.6574	2.3783	29.3%	6.7493	1.7401	31.5420	2.2159	27.6%	12.4465	2.2104



Fig. 7: Different methods for cross-view image translation task in 256×256 resolution on CVUSA dataset.

to improve the structure accuracy since the controllable structure can provide a strong supervision to the discriminator. The proposed controllable structure guided self-identity preserving loss can push the generated data distribution close to the real data distribution. Finally, the perceptual loss and the total variation loss aim to improve the image fidelity.

Ablation Analysis. The results of ablation study are shown in Table I. We observe that Baseline B is better than baseline A since the ground truth image y can provide a strong supervised information to the generator G . Comparing Baseline B with Baseline C, the controllable structure guided generation improves the performance on all metrics by large margins, which confirms that the controllable structures can provide more structural information to the generator G . By using the proposed controllable structure guided cycle, Baseline D further improves over baseline C, meaning that the cycle structure indeed utilizes the controllable structure information in a more effective way, confirming our design motivation. Baseline E12 outperforms baseline D which uses the $L1$ loss on SSIM, PSNR and SD metrics showing the importance of using the proposed color loss to avoid the “channel pollution” issue. By

further combining the color $L1$ loss and the $L1$ loss on the generated image y' , we can further improve the performance as shown in baseline E14. However, replacing the color $L1$ loss with the color $L2$ loss will degrade the performance as shown by baseline E13 but the results are still better than using baseline D. We also use the proposed color loss on the reconstructed image x' as presented in baseline E11, but it achieves worst results. Comparing Baseline D with Baseline E21, the proposed controllable structure guide discriminator improves the top-1 accuracy by 0.65 and 1.98, which confirms the importance of our design motivation. By further combining the controllable structure guide discriminator with the traditional discriminator in baseline E22, both top-1 and top-5 accuracies are further boosted. Baseline E3 outperforms D with around 0.13 points gain on the KL metric, clearly demonstrating the effectiveness of the proposed controllable structure guided self-identity preserving loss. By adding the perceptual loss and the TV loss in baseline E4x, the overall performance is further improved on LPIPS metric [46], which uses pretrained deep models to evaluate the similarity and highly agrees with human perception. Finally, we demonstrate the advantage of the proposed full model in baseline F, which integrates baseline D, E14, E22, E3 and E42. It is obvious that baseline F achieves the best results on both accuracy and KL score metrics. However, we observe that baseline F achieves worse results on SSIM, PSNR and SD compared with baseline E14, and at the same time it achieves worse results on LPIPS metric compared with baseline E42. This is also observed in LPIPS [46], i.e., the traditional metrics (i.e., SSIM, PSNR, SD, FSIM) disagree with metrics based on deep architectures such as VGG [34]. Thus, we try to balance both metrics to a reasonable results without dropping significantly the performance, and we still observe that baseline F achieves

TABLE VII: Quantitative evaluation of Dayton dataset in 64×64 resolution. For all metrics except KL score, higher is better. (*, †) These results are reported in [10] and [9], respectively. (‡) Inception Score for real (ground truth) data in the a2g direction is 2.3534, 1.8135 and 2.3250 for all, top-1 and top-5 setups, respectively. Inception Score for real data in g2a direction is 2.3015, 1.5056 and 2.2095 for all, top-1 and top-5 setups, respectively.

Dir.	Method	Accuracy (%)				Inception Score [‡]			SSIM	PSNR	SD	KL
		Top-1		Top-5		all	Top-1	Top-5				
a2g	Pix2pix [2]	7.90*	15.33*	27.61*	39.07*	1.8029*	1.5014*	1.9300*	0.4808*	19.4919*	16.4489*	$6.29 \pm 0.80^*$
	X-Fork [10]	16.63*	34.73*	46.35*	70.01*	1.9600*	1.5908*	2.0348*	0.4921*	19.6273*	16.4928*	$3.42 \pm 0.72^*$
	X-Seq [10]	4.83*	5.56*	19.55*	24.96*	1.8503*	1.4850*	1.9623*	0.5171*	20.1049*	16.6836*	$6.22 \pm 0.87^*$
	SelectionGAN [9]	45.37†	79.00†	83.48†	97.74†	2.1606†	1.7213†	2.1323†	0.6865†	24.6143†	18.2374†	$1.70 \pm 0.45†$
	Ours	49.86	84.41	86.14	99.61	2.1059	1.7342	2.0737	0.6754	24.2814	18.1361	1.54 ± 0.39
g2a	Pix2pix [2]	1.65*	2.24*	7.49*	12.68*	1.7970*	1.3029*	1.6101*	0.3675*	20.5135*	14.7813*	$6.39 \pm 0.90^*$
	X-Fork [10]	4.00*	16.41*	15.42*	35.82*	1.8557*	1.3162*	1.6521*	0.3682*	20.6933*	14.7984*	$4.45 \pm 0.84^*$
	X-Seq [10]	1.55*	2.99*	6.27*	8.96*	1.7854*	1.3189*	1.6219*	0.3663*	20.4239*	14.7657*	$7.20 \pm 0.92^*$
	SelectionGAN [9]	14.12†	51.81†	39.45†	74.70†	2.1571†	1.4441†	2.0828†	0.5118†	23.2657†	16.2894†	$2.25 \pm 0.56†$
	Ours	16.65	44.83	44.03	77.01	2.0802	1.4360	2.0628	0.5064	23.3632	16.4788	2.16 ± 0.59

TABLE VIII: Quantitative evaluation of Dayton dataset in 256×256 resolution. For all metrics except KL score, higher is better. (*, †) These results are reported in [10] and [9], respectively. (‡) Inception Score for real (ground truth) data in the a2g direction is 3.8319, 2.5753 and 3.9222 for all, top-1 and top-5 setups, respectively. Inception Score for real data in g2a direction is 3.7196, 2.3626 and 3.8998 for all, top-1 and top-5 setups, respectively.

Dir.	Method	Accuracy (%)				Inception Score [‡]			SSIM	PSNR	SD	KL
		Top-1		Top-5		all	Top-1	Top-5				
a2g	Pix2pix [2]	6.80*	9.15*	23.55*	27.00*	2.8515*	1.9342*	2.9083*	0.4180*	17.6291*	19.2821*	$38.26 \pm 1.88^*$
	X-Fork [10]	30.00*	48.68*	61.57*	78.84*	3.0720*	2.2402*	3.0932*	0.4963*	19.8928*	19.4533*	$6.00 \pm 1.28^*$
	X-Seq [10]	30.16*	49.85*	62.59*	80.70*	2.7384*	2.1304*	2.7674*	0.5031*	20.2803*	19.5258*	$5.93 \pm 1.32^*$
	SelectionGAN [9]	42.11†	68.12†	77.74†	92.89†	3.0613†	2.2707†	3.1336†	0.5938†	23.8874†	20.0174†	$2.74 \pm 0.86†$
	Ours	49.12	80.43	81.20	94.87	3.3210	2.3494	3.3522	0.5633	23.3515	19.7692	2.17 ± 0.77
g2a	Pix2pix [2]	10.23*	16.02*	30.90*	40.49*	3.5676*	2.0325*	2.8141*	0.2693*	20.2177*	16.9477*	$7.88 \pm 1.24^*$
	X-Fork [10]	10.54*	15.29*	30.76*	37.32*	3.1342*	1.8656*	2.5599*	0.2763*	20.5978*	16.9962*	$6.92 \pm 1.15^*$
	X-Seq [10]	12.30*	19.62*	35.95*	45.94*	3.5849*	2.0489*	2.8414*	0.2725*	20.2925*	16.9285*	$7.07 \pm 1.19^*$
	SelectionGAN [9]	20.66†	33.70†	51.01†	63.03†	3.2446†	2.1331†	3.4091†	0.3284†	21.8066†	17.3817†	3.55 ± 0.87†
	Ours	17.31	29.40	43.58	55.27	3.2131	2.0916	3.3637	0.3357	22.0273	17.6542	5.17 ± 1.23

TABLE IX: Quantitative evaluation of CVUSA dataset in the a2g direction. For all metrics except KL score, higher is better. (*, †) These results are reported in [10] and [9], respectively. (‡) Inception Score for real (ground truth) data is 4.8741, 3.2959 and 4.9943 for all, top-1 and top-5 setups, respectively.

Method	Accuracy (%)				Inception Score [‡]			SSIM	PSNR	SD	KL
	Top-1		Top-5		all	Top-1	Top-5				
Zhai et al. [45]	13.97*	14.03*	42.09*	52.29*	1.8434*	1.5171*	1.8666*	0.4147*	17.4886*	16.6184*	$27.43 \pm 1.63^*$
Pix2pix [2]	7.33*	9.25*	25.81*	32.67*	3.2771*	2.2219*	3.4312*	0.3923*	17.6578*	18.5239*	$59.81 \pm 2.12^*$
X-Fork [10]	20.58*	31.24*	50.51*	63.66*	3.4432*	2.5447*	3.5567*	0.4356*	19.0509*	18.6706*	$11.71 \pm 1.55^*$
X-Seq [10]	15.98*	24.14*	42.91*	54.41*	3.8151*	2.6738*	4.0077*	0.4231*	18.8067*	18.4378*	$15.52 \pm 1.73^*$
SelectionGAN [9]	41.52†	65.51†	74.32†	89.66†	3.8074†	2.7181†	3.9197†	0.5323†	23.1466†	19.6100†	$2.96 \pm 0.97†$
Ours	45.06	70.04	78.31	93.47	3.9469	2.8779	4.0383	0.5366	22.8223	19.8276	2.60 ± 0.97

TABLE X: LPIPS of SelectionGAN [9] and ours for cross-view image translation task. For this metric, lower is better.

Dir.	Method	Dayton (64×64)		Dayton (256×256)	CVUSA
		Top-1	Top-5		
a2g	SelectionGAN [9]	0.1786		0.4996	0.4652
	Ours	0.1712		0.3529	0.3817
g2a	SelectionGAN [9]	0.2489		0.5264	-
	Ours	0.2382		0.4527	-

better performance on all SSIM, PSNR, SD and LPIPS metrics than baseline D.

Hyper-parameter Analysis. (i) For cross-view image translation task, we investigate the influence of λ_{cyc} , λ_{id} , λ_{vgg} to the performance of our model. The results are shown in Tables II, III and IV. In Table II, when λ_{cyc} becomes smaller, we achieve better results on most metrics.

This means that adjusting the ratio of weighting parameters of the cycle can obtain further performance improvement. This is different from CycleGAN [11], which uses the same weights for both forward and backward cycle-consistency losses since

CycleGAN tries to learning two mappings, while in our model we only focus on generating photo-realistic y' and do not care about the quality of the reconstructed image x'' . Thus, the forward part has a larger weight than the backward part. Moreover, we also investigate the influence of λ_{id} and λ_{vgg} . The results are listed in Tables III and IV. When both λ_{id} and λ_{vgg} become bigger, the generator with a larger error loss dominates the training, making the whole model generating better results. Therefore, we empirically set $\lambda_{cyc}=0.1$, $\lambda_{id}=100$, $\lambda_{vgg}=100$, $\lambda_{color}=100$ and $\lambda_{tv}=1e-6$ in Eq. (14) for this task. (ii) For hand gesture-to-gesture translation task, we empirically set $\lambda_{cyc}=0.1$, $\lambda_{id}=0.01$, $\lambda_{vgg}=1000$, $\lambda_{color}=800$ and $\lambda_{tv}=1e-6$ in Eq. (14) for this task. Moreover, we also investigate the influence of the number of cycles on this task. Results are shown in Table V and we observe that the two-cycle solution achieves better results than one-cycle on most metrics.

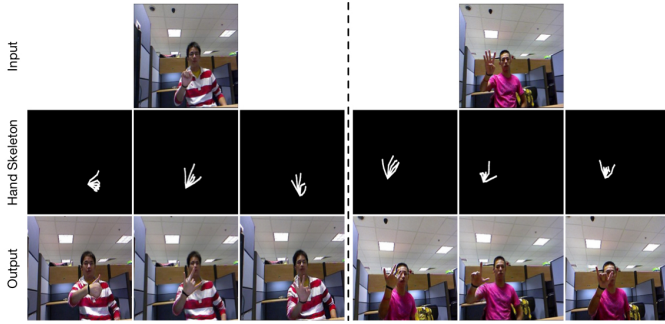


Fig. 8: Arbitrary hand gesture-to-gesture translation of our model.

C. Hand Gesture-to-Gesture Translation

State-of-the-Art Comparisons. We compare the proposed model with the most related works, i.e., PG² [4], SAMG [7], PoseGAN [8], DPIG [6] and GestureGAN [22]. PG² and DPIG try to generate a person image with different poses based on conditional person images and target keypoints. SAMG and PoseGAN explicitly employ human skeleton information to generate person images. Note that SAMG adopts a CGAN to generate motion sequences based on appearance information and skeleton information by exploiting frame level smoothness. We re-implemented this model to generate a single frame for fair comparison. These methods are paired image-to-image models and comparison results are shown in Fig. 4 and 5. As we can see in both figures, the proposed model consistently produces sharper images with convincing details compared with other baselines on both datasets. We also note that the proposed GAN model is more robust than existing methods as shown in the first row of Fig. 4. Existing methods are easy to overfit since they generate the dropping arm as shown in the white dotted box while the proposed model failed to generate it. It is hard to generate the dropping arm since no guidance has been provided to generate it, while existing methods just simply memorize the blocks from training images to generate new ones rather than to learn the representations between different images. Moreover, we also provide quantitative results in Table VI, and we can see that the proposed GAN model produces more photo-realistic results than other baselines on all metrics except IS. This phenomenon can also be observed in PG² [4], GestureGAN [22] and other super-resolution works such as [33], i.e., sharper results have a lower IS. Finally, we also show some results of the arbitrary hand gesture-to-gesture translation on NTU Hand Digit dataset in Fig. 8. Given a single image and several hand skeletons, the proposed model can generate the corresponding hand gestures.

User Study. We also conducted a user study similar to [4], [11], [8]. We follow the same settings as in [2] to perform an Amazon Mechanical Turk (AMT) perceptual study. The results on NTU Hand Digit and Senz3D datasets compared with the baseline models are shown in Table VI. We observe that the proposed model consistently achieves the best performance compared with these baselines.

FID v.s. FRD. We also compare the performance between FID and the proposed FRD metric. The results are shown in Table VI and we can observe that FRD is more consistent with

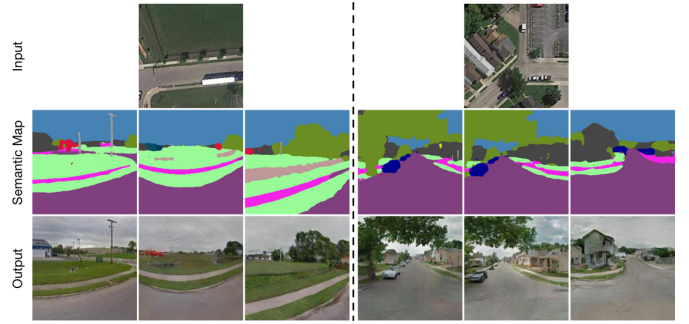


Fig. 9: Arbitrary cross-view image translation of our model.

the human judgment, i.e., the AMT score, than the FID metric. Moreover, we observe that the difference in FRD between GestureGAN and the other methods is not as obvious as in the results from the user study, i.e., the AMT metric. The reason is that FRD calculates the Fréchet distance between the feature maps extracted from the real image and the generated image using CNNs which are trained with semantic labels. Thus, these feature maps are employed to reflect the semantic distance between the images. The semantic distance between the images is not very large considering they are all hands. On the contrary, the user study measures the generation quality from a perceptual level. The difference on the perceptual level is more obvious than on the semantic level, i.e., the generated images with small artifacts show minor differences on the feature level, while are being judged with a significant difference from the real images by humans.

D. Cross-View Image Translation

State-of-the-art Comparison. We compare the proposed model with five recently proposed state-of-the-art methods on the cross-view image translation task, i.e., Pix2pix [2], Zhai et al. [45], X-Fork [10], X-Seq [10] and SelectionGAN [9]. The comparison results are shown in Tables VII, VIII, IX and X. We can observe the significant improvement of the proposed model in these tables. The proposed model consistently outperforms Pix2pix, Zhai et al., X-Fork and X-Seq on all the metrics. Moreover, comparing against SelectionGAN, the proposed model still achieves competitive performance on all metrics excepting SSIM, PSNR and SD. In most cases of the a2g direction in Tables VII and VIII we achieve a slightly lower performance as compared with SelectionGAN. However, we consistently achieve better performance than SelectionGAN on LPIPS metric as shown in Table X, which agrees more with human judgments as indicated in [46]. Finally, we also note that SelectionGAN is carefully designed for the cross-view image translation task while the proposed model is a generic framework.

Qualitative Evaluation. The qualitative results in higher resolution on Dayton and CVUSA datasets are shown in Fig. 6 and 7. The proposed model generates better results against other baselines in terms of detail preservation and translation visual effects. In addition, it can be seen that our method generates more clear details on objects/scenes such as road, trees, clouds than SelectionGAN in the generated ground level images (zoom-in for details in Fig. 6). For the generated aerial

TABLE XI: Comparison of the number of network parameters on cross-view image translation task.

Model	Pix2pix [2]	X-Fork [10]	X-Seq [10]	SelectionGAN [9]	Ours
<i>G</i>	39.0820 M	39.2163 M	39.0820*2 M	55.4808 M	11.3876 M
<i>D</i>	2.7696 M	2.7696 M	2.7696*2 M	2.7687 M	2.7678+2.7709 M
Total	41.8516 M	41.9859 M	83.7032 M	58.2495 M	16.9263 M

images, we can observe that grass, trees and house roofs are well rendered compared to others. Moreover, the results generated by our method are closer to the ground truth in layout and structure (see the results in the a2g direction in Fig. 6 and 7).

Arbitrary Cross-View Image Translation. Existing methods such as Zhai et al. [45], Pix2pix [2], X-Fork [10] and X-Seq [10] focus on the cross-view image translation task. However, this task is essentially an ill-posed problem and has limited scalability and robustness in handling more than two viewpoints. A recent work SelectionGAN [9] extends the cross-view image translation task to a more generic task of the problem, i.e., the arbitrary cross-view image translation, in which a single input view can be translated to different target views. For the arbitrary cross-view image translation, conditional labels are usually required since learning an one-to-many mapping is more challenging and extremely hard to optimize. Similarly to the arbitrary hand gesture-to-gesture translation in Fig. 8, we show several results of arbitrary cross-view image translation task on Dayton dataset in Fig. 9. We believe this task have many applications such as cross-view image geo-localization.

Network Parameter Comparisons. We compare the overall network parameter with Pix2pix [2], X-Fork [10], X-Seq [10] and SelectionGAN [9] on cross-view image translation task. Results are shown in Table XI. As we can see, the proposed model achieves superior model capacity and produces better generation performance comparing with existing models.

V. CONCLUSIONS

In this paper, we focus on the challenging task of controllable image-to-image translation. To this end, we propose a unified GAN framework, which can generate target images with different poses, sizes, structures and locations based on a conditional image and controllable structures. In this way, the conditional image can provide appearance information and the controllable structures can provide structure information for generating the final results. Moreover, we also propose three novel losses to learn the mapping from the source domain to the target domain, i.e., color loss, controllable structure guided cycle-consistency loss and controllable structure guided self-identity preserving loss. It is worth noting that the proposed color loss handles the “channel pollution” problem when back-propagating the gradients, which frequently occurs in the existing generative models. The controllable structure guided cycle-consistency loss can reduce the dis-match between the source domain and the target domain. The controllable structure guided self-identity preserving loss aims to preserve the identity information of the generated images. In addition, we present a novel Fréchet ResNet Distance (FRD) metric to evaluate the quality of generated images. Experimental results show that the proposed unified GAN framework achieves

competitive performance compared with the state of the art using carefully designed frameworks on two challenging generative tasks, i.e., hand gesture-to-gesture translation and cross-view image translation. Note that the proposed GAN framework is not tuned to any specific controllable image-to-image translation tasks.

Acknowledgments. This work is partially supported by National Natural Science Foundation of China (NSFC, No.U1613209,61673030), Shenzhen Key Laboratory for Intelligent Multimedia and Virtual Reality (ZDSYS201703031405467).

REFERENCES

- [1] D. Pathak, P. Krahenbuhl, J. Donahue, T. Darrell, and A. A. Efros, “Context encoders: Feature learning by inpainting,” in *CVPR*, 2016. **2, 5**
- [2] P. Isola, J.-Y. Zhu, T. Zhou, and A. A. Efros, “Image-to-image translation with conditional adversarial networks,” in *CVPR*, 2017. **1, 2, 3, 4, 5, 6, 8, 10, 11, 12**
- [3] J.-Y. Zhu, R. Zhang, D. Pathak, T. Darrell, A. A. Efros, O. Wang, and E. Shechtman, “Toward multimodal image-to-image translation,” in *NIPS*, 2017. **1, 2, 3**
- [4] L. Ma, X. Jia, Q. Sun, B. Schiele, T. Tuytelaars, and L. Van Gool, “Pose guided person image generation,” in *NIPS*, 2017. **1, 2, 3, 4, 5, 6, 7, 9, 11**
- [5] L. Song, Z. Lu, R. He, Z. Sun, and T. Tan, “Geometry guided adversarial facial expression synthesis,” in *ACM MM*, 2018. **1, 2**
- [6] L. Ma, Q. Sun, S. Georgoulis, L. Van Gool, B. Schiele, and M. Fritz, “Disentangled person image generation,” in *CVPR*, 2018. **1, 2, 3, 9, 11**
- [7] Y. Yan, J. Xu, B. Ni, W. Zhang, and X. Yang, “Skeleton-aided articulated motion generation,” in *ACM MM*, 2017. **1, 2, 3, 9, 11**
- [8] A. Siarohin, E. Sangineto, S. Lathuiliere, and N. Sebe, “Deformable gans for pose-based human image generation,” in *CVPR*, 2018. **1, 2, 3, 4, 9, 11**
- [9] H. Tang, D. Xu, N. Sebe, Y. Wang, J. J. Corso, and Y. Yan, “Multi-channel attention selection gan with cascaded semantic guidance for cross-view image translation,” in *CVPR*, 2019. **1, 2, 3, 4, 8, 10, 11, 12**
- [10] K. Regmi and A. Borji, “Cross-view image synthesis using conditional gans,” in *CVPR*, 2018. **1, 2, 3, 4, 6, 7, 10, 11, 12**
- [11] J.-Y. Zhu, T. Park, P. Isola, and A. A. Efros, “Unpaired image-to-image translation using cycle-consistent adversarial networks,” in *ICCV*, 2017. **1, 2, 3, 4, 5, 6, 8, 10, 11**
- [12] T. Kim, M. Cha, H. Kim, J. Lee, and J. Kim, “Learning to discover cross-domain relations with generative adversarial networks,” in *ICML*, 2017. **1, 2, 3**
- [13] Z. Yi, H. Zhang, P. Tan, and M. Gong, “Dualgan: Unsupervised dual learning for image-to-image translation,” in *ICCV*, 2017. **1, 2, 3**
- [14] A. Anoosheh, E. Agustsson, R. Timofte, and L. Van Gool, “Combogan: Unrestrained scalability for image domain translation,” in *CVPR Workshops*, 2018. **1, 2, 3**
- [15] H. Tang, D. Xu, W. Wang, Y. Yan, and N. Sebe, “Dual generator generative adversarial networks for multi-domain image-to-image translation,” in *ACCV*, 2018. **1, 2, 3**
- [16] Y. Choi, M. Choi, M. Kim, J.-W. Ha, S. Kim, and J. Choo, “Stargan: Unified generative adversarial networks for multi-domain image-to-image translation,” in *CVPR*, 2018. **1, 2, 3, 4**
- [17] I. Goodfellow, J. Pouget-Abadie, M. Mirza, B. Xu, D. Warde-Farley, S. Ozair, A. Courville, and Y. Bengio, “Generative adversarial nets,” in *NIPS*, 2014. **1, 3, 6**
- [18] T. Karras, S. Laine, and T. Aila, “A style-based generator architecture for generative adversarial networks,” in *CVPR*, 2019. **1, 3**
- [19] A. Brock, J. Donahue, and K. Simonyan, “Large scale gan training for high fidelity natural image synthesis,” in *ICLR*, 2019. **1, 3**
- [20] M. Mirza and S. Osindero, “Conditional generative adversarial nets,” *arXiv preprint:1411.1784*, 2014. **1**
- [21] S. E. Reed, Z. Akata, S. Mohan, S. Tenka, B. Schiele, and H. Lee, “Learning what and where to draw,” in *NIPS*, 2016. **1, 3**
- [22] H. Tang, W. Wang, D. Xu, Y. Yan, and N. Sebe, “Gesturegan for hand gesture-to-gesture translation in the wild,” in *ACM MM*, 2018. **1, 3, 6, 7, 9, 11**
- [23] T. Park, M.-Y. Liu, T.-C. Wang, and J.-Y. Zhu, “Semantic image synthesis with spatially-adaptive normalization,” in *CVPR*, 2019. **1, 3**

- [24] T.-C. Wang, M.-Y. Liu, J.-Y. Zhu, A. Tao, J. Kautz, and B. Catanzaro, "High-resolution image synthesis and semantic manipulation with conditional gans," in *CVPR*, 2018. 1, 3, 5
- [25] T.-C. Wang, M.-Y. Liu, J.-Y. Zhu, G. Liu, A. Tao, J. Kautz, and B. Catanzaro, "Video-to-video synthesis," in *NeurIPS*, 2018. 3
- [26] A. Siarohin, S. Lathuilière, S. Tulyakov, E. Ricci, and N. Sebe, "Animating arbitrary objects via deep motion transfer," in *CVPR*, 2019. 3
- [27] W. Xian, P. Sangkloy, V. Agrawal, A. Raj, J. Lu, C. Fang, F. Yu, and J. Hays, "Texturegan: Controlling deep image synthesis with texture patches," in *CVPR*, 2018. 3
- [28] T. Qiao, J. Zhang, D. Xu, and D. Tao, "Mirrorgan: Learning text-to-image generation by redescription," in *CVPR*, 2019. 3
- [29] H. Tang, X. Chen, W. Wang, D. Xu, J. J. Corso, N. Sebe, and Y. Yan, "Attribute-guided sketch generation," in *FG*, 2019. 3
- [30] W. Chen and J. Hays, "Sketchygan: Towards diverse and realistic sketch to image synthesis," in *CVPR*, 2018. 3
- [31] H. Tang, D. Xu, G. Liu, W. Wang, N. Sebe, and Y. Yan, "Cycle in cycle generative adversarial networks for keypoint-guided image generation," in *ACM MM*, 2019. 3
- [32] Z. Cao, T. Simon, S.-E. Wei, and Y. Sheikh, "Realtime multi-person 2d pose estimation using part affinity fields," in *CVPR*, 2017. 4
- [33] J. Johnson, A. Alahi, and L. Fei-Fei, "Perceptual losses for real-time style transfer and super-resolution," in *ECCV*, 2016. 5, 6, 11
- [34] K. Simonyan and A. Zisserman, "Very deep convolutional networks for large-scale image recognition," in *ICLR*, 2015. 5, 9
- [35] T. Nguyen, T. Le, H. Vu, and D. Phung, "Dual discriminator generative adversarial nets," in *NIPS*, 2017. 6
- [36] D. Kingma and J. Ba, "Adam: A method for stochastic optimization," in *ICLR*, 2015. 6
- [37] T. Simon, H. Joo, I. Matthews, and Y. Sheikh, "Hand keypoint detection in single images using multiview bootstrapping," in *CVPR*, 2017. 6
- [38] G. Lin, A. Milan, C. Shen, and I. Reid, "Refinenet: Multi-path refinement networks for high-resolution semantic segmentation," in *CVPR*, 2017. 6
- [39] Z. Ren, J. Yuan, J. Meng, and Z. Zhang, "Robust part-based hand gesture recognition using kinect sensor," *IEEE TMM*, vol. 15, no. 5, pp. 1110–1120, 2013. 6
- [40] A. Memo and P. Zanuttigh, "Head-mounted gesture controlled interface for human-computer interaction," *Springer MTA*, pp. 1–27, 2016. 6
- [41] N. N. Vo and J. Hays, "Localizing and orienting street views using overhead imagery," in *ECCV*, 2016. 6
- [42] S. Workman, R. Souvenir, and N. Jacobs, "Wide-area image geolocalization with aerial reference imagery," in *ICCV*, 2015. 6
- [43] M. Heusel, H. Ramsauer, T. Unterthiner, B. Nessler, G. Klambauer, and S. Hochreiter, "Gans trained by a two time-scale update rule converge to a nash equilibrium," in *NIPS*, 2017. 7
- [44] H. Tang and H. Liu, "A novel feature matching strategy for large scale image retrieval," in *IJCAI*, 2016. 7
- [45] M. Zhai, Z. Bessinger, S. Workman, and N. Jacobs, "Predicting ground-level scene layout from aerial imagery," in *CVPR*, 2017. 10, 11, 12
- [46] R. Zhang, P. Isola, A. A. Efros, E. Shechtman, and O. Wang, "The unreasonable effectiveness of deep features as a perceptual metric," in *CVPR*, 2018. 9, 11